Journal of Pharmaceutical Analysis 14 (2024) 100956

Contents lists available at ScienceDirect

Journal of Pharmaceutical Analysis

journal homepage: www.elsevier.com/locate/jpa

Original article

Oxalate regulates crystal-cell adhesion and macrophage metabolism via JPT2/PI3K/AKT signaling to promote the progression of kidney stones

Qianlin Song [a, 1], Chao Song [a, 1], Xin Chen [b, 1], Yunhe Xiong [a], Ziqi He [a], Xiaozhe Su [a], Jiawei Zhou [a], Hu Ke [a], Caitao Dong [a], Wenbiao Liao [a, **], Sixing Yang [a, *]

[a] Department of Urology, Renmin Hospital of Wuhan University, Wuhan, 430060, China
[b] Department of Obstetrics and Gynecology, Renmin Hospital of Wuhan University, Wuhan, 430060, China

ARTICLE INFO

Article history:
Received 25 September 2023
Received in revised form
7 February 2024
Accepted 21 February 2024
Available online 27 February 2024

Keywords:
Oxalate
Kidney stones
JPT2
Crystal-cell adhesion
Immunoregulation

ABSTRACT

Oxalate is an organic dicarboxylic acid that is a common component of plant foods. The kidneys are essential organs for oxalate excretion, but excessive oxalates may induce kidney stones. Jupiter microtubule associated homolog 2 (JPT2) is a critical molecule in Ca^{2+} mobilization, and its intrinsic mechanism in oxalate exposure and kidney stones remains unclear. This study aimed to reveal the mechanism of JPT2 in oxalate exposure and kidney stones. Genetic approaches were used to control JPT2 expression in cells and mice, and the JPT2 mechanism of action was analyzed using transcriptomics and untargeted metabolomics. The results showed that oxalate exposure triggered the upregulation of JPT2, which is involved in nicotinic acid adenine dinucleotide phosphate (NAADP)-mediated Ca^{2+} mobilization. Transcriptomic analysis revealed that cell adhesion and macrophage inflammatory polarization were inhibited by JPT2 knockdown, and these were dominated by phosphatidylinositol 3-kinase (PI3K)/AKT signaling, respectively. Untargeted metabolomics indicated that JPT2 knockdown inhibited the production of succinic acid semialdehyde (SSA) in macrophages. Furthermore, JPT2 deficiency in mice inhibited kidney stones mineralization. In conclusion, this study demonstrates that oxalate exposure facilitates kidney stones by promoting crystal-cell adhesion, and modulating macrophage metabolism and inflammatory polarization via JPT2/PI3K/AKT signaling.

1. Introduction

Oxalate is present in a wide range of plant foods (fruits, vegetables, nuts, legumes, etc.), which makes it difficult for humans to avoid exposure to oxalate [1]. Oxalate has a positive role in industrial production and is often used as a raw material for certain drugs, bleach, detergents, plastics, etc. [2–4]. However, in the human body, supraphysiologic concentrations of oxalate are usually considered a harmful substance [1]. The vast majority of oxalate absorbed into the bloodstream from the diet or produced endogenously is excreted by the kidneys [5,6]. Excess oxalate leads to hyperoxaluria, which increases the risk of calcium oxalate kidney stones [6].

Kidney stones are a globally prevalent urological disease. The high incidence, high recurrence rate, and high percentage of hospitalization structure of kidney stones contribute to a severe health insurance burden [7,8]. Kidney stones have significant regional specificity and environmental relevance. It has been reported that areas with higher concentrations of oxalate in the soil and drinking water environment tend to have a higher incidence of kidney stones [9]. However, the mechanism of oxalate and kidney stones mineralization is still not fully elucidated.

Jupiter microtubule-associated homolog 2 (JPT2) has recently been identified as a binding protein for nicotinic acid adenine dinucleotide phosphate (NAADP) [10]. NAADP is currently the most effective second messenger for endogenous Ca^{2+} mobilization. Upon specific stimulation, cells rapidly produce NAADP and upregulate JPT2 expression, which together form a functional complex, ultimately triggering Ca^{2+} release [11,12].

* Corresponding author.
** Corresponding author.
E-mail addresses: liaowenbiao@whu.edu.cn (W. Liao), sxyang@whu.edu.cn (S. Yang).
[1] These authors contributed equally to this work and share the first authorship.

https://doi.org/10.1016/j.jpha.2024.02.010

Ca^{2+} is a widespread and vital intracellular signal regulating various physiological and pathological cell processes [13]. Evidence suggests that Pb^{2+}-induced Ca^{2+} release is an important factor in initiating calcium oxalate crystal formation and nucleation [14]. However, the function of JPT2, a critical factor for endogenous Ca^{2+} mobilization, in oxalate and kidney stones mineralization is unclear.

It reports new findings that oxalate exposure is involved in the mechanism of kidney stones mineralization through activation of the JPT2/phosphatidylinositol 3-kinase (PI3K)/AKT signaling. These findings are vitally important for enriching the mechanism of kidney stones mineralization and exploring drug targets for kidney stones therapy.

2. Materials and methods

The Materials and Methods section is described in the Supplementary Materials [1,15–20].

3. Results

3.1. Oxalate increases the abundance of JPT2 expression in renal tubular epithelial cells (RTEC) and mice kidneys

First, we sought to determine the expression pattern of JPT2 in response to oxalate exposure. We examined Ca^{2+} levels in the glyoxylate (Gly)-constructed *in vivo* kidney stones model and the oxalate-constructed *in vitro* kidney stones model. Von kossa staining showed the successful establishment of the kidney stones model induced by Gly (Fig. 1A). Subsequently, it was found that Ca^{2+} concentration was significantly increased in the *in vitro* kidney stones model constructed with Gly (Fig. 1B), and the *in vivo* kidney stones model constructed with oxalate Fig. S1A, B(Figs. 1C and D and Fig. S1A and B). There was a positive correlation (Fig. 1E) between calcium oxalate deposition and the degree of Ca^{2+} accumulation in the kidneys. Then, the results of enzyme-linked immunosorbent assay (ELISA) found that the content of NAADP was significantly increased in the *in vitro* kidney stones model constructed with Gly (Fig. 1F) and the *in vivo* kidney stones model constructed with oxalate Fig. S1C(Figs. 1G and S1C). Pearson correlation analysis found a positive correlation between NAADP and Ca^{2+} concentration in the kidney stones model (Figs. 1H, 1I and S1D). The currently identified NAADP binding proteins are JPT2 and like-Sm protein 12 (LSM12) [12]. Therefore, to confirm the binding proteins in which NAADP exerts Ca^{2+} mobilization in kidney stone formation, we examined the expression of JPT2 and LSM12. As shown in (Fig. 1J, 1K and S1E), the expression of JPT2 was significantly increased in the kidney stones models, and the expression of JPT2 peaked after 24 h, while the expression of LSM12 was not significantly different. Immediately after, to further determine whether the upregulation of JPT2 was triggered by NAADP, we downregulated NAADP and observed JPT2 expression. CD38, dual oxidase 1 (DUOX1), and dual oxidase 2 (DUOX2) are common NAADP synthases [21,22]. Thus, we examined the expression of DUOX1, DUOX2, and CD38 in kidney stones. The results showed that both protein (Figs. 1L, 1M and S1F) and mRNA Fig. S1G, H(Figs. S1G and H) expression of DUOX1 and CD38 were significantly upregulated in kidney stones, whereas no significant changes were observed in DUOX2. Compound 78c [23] and diphenyleneiodonium chloride [24] are potent inhibitors of CD38 and DUOX1, respectively. The results of ELISA revealed that compound 78c significantly inhibited the expression of NAADP in kidney stones, whereas diphenyleneiodonium chloride had no significant effect (Fig. S1I and J). Hence, compound 78c was used to hinder the production of NAADP. As shown in (Figs. 1N–P, and S1K and L), inhibition of NAADP production significantly restricts the accumulation of Ca^{2+} in the kidney stones models. Also, the expression of JPT2 was restricted (Figs. 1Q, 1R and S1M). These data suggested that oxalate exposure stimulated an increase in NAADP and upregulated JPT2 expression, which triggered Ca^{2+} mobilization within RTEC, which may be involved in the pathological process of kidney stones formation.

3.2. JPT2 promotes crystal-cell adhesion caused by oxalate exposure

To determine whether JPT2 has an important function in oxalate exposure on kidney stones mineralization. First, we have generated the *JPT2* knockdown in HK-2 cells by short hairpin (sh) -JPT2 lentivirus (Fig. S2A). Immediately after, RNA-seq was used to analyze the differential genes expression and functional enrichment following *JPT2* knockdown in HK-2 cells under oxalate intervention. As shown in (Fig. 2A), significant differential genes were screened for |log2 fold change (FC)| $\geq$ 1 and false discovery rate (FDR) $\leq$ 0.05. 719 genes were down-regulated, and 839 genes were up-regulated in the oxalate (Ox) + sh-JPT2 group compared to the Ox + control (Ctrl)-sh group. The results of gene ontology (GO) analysis (Fig. 2B) observed that the biological processes of cell adhesion and biological adhesion were significantly enriched. Therefore, in order to estimate the position of JPT2 in crystal-cell adhesion, we performed the knockdown and overexpression of *JPT2* in HK-2 and HEK-293 cells (Figs. S2B–D). The results of cell adhesion capacity (Figs. 2C and D) and crystal adhesion assay (Figs. 2E–G) showed that overexpression of *JPT2* enhanced the adhesion capacity of cells, but knockdown of *JPT2* had the opposite effect. Subsequently, the Kyoto Encyclopedia of Genes and Genomes (KEGG) enrichment analysis (Fig. 2H) showed that cell adhesion molecules were significantly enriched. Next, it was revealed that vascular cell adhesion molecule 1 (VCAM1) was the most significant differential gene in cell adhesion molecules (Fig. 2I). VCAM1 is a vital cell adhesion molecule involved in cell-cell or extracellular matrix adhesion and interactions [25,26]. Therefore, we examined the expression of VCAM1 in the kidney stones model. As shown in (Figs. 2J–N), The mRNA and protein expression of VCAM1 in HK-2 cells and HEK-293 cells was upregulated by oxalate intervention. *JPT2* overexpression exacerbated the mRNA and protein expression of VCAM1, whereas *JPT2* knockdown attenuated the expression of VCAM1. Next, to verify whether the crystal adhesion effect of JPT2 was through VCAM1, we overexpressed *VCAM1* on HK-2 and HEK-293 cells (Figs. S2E and F). Then, we proceeded to examine the cell adhesion ability and crystal-cell adhesion. The results of cell adhesion capacity (Figs. 2O and P) and crystal adhesion assay (Figs. 2Q–S) showed that overexpression of *VCAM1* reversed the cell adhesion capacity weakened by the deficiency of JPT2. Thus, these data suggested that JPT2 promotes crystal-cell adhesion resulting from oxalate exposure and that VCAM1 may be necessary for this.

3.3. JPT2 promotes oxalate-induced macrophage chemotaxis and inflammatory polarization

The exchange of inflammatory signals between macrophages, as immune cells of the body, and RTEC is an essential connection in the pathogenesis of kidney stones [27]. To further investigate the effect of JPT2 on communication between RTEC and macrophages, the conditioned medium (CM) for RTEC was used to intervene with M0 macrophages induced by phorbol-12-myristate-13-acetate (PMA) (Fig. 3A). The results of the macrophage chemotaxis assay (Figs. 3B and C, and S3A and B) showed that the CM derived from HK-2 and HEK-293 cells after oxalate intervention enhanced macrophage chemotaxis. Moreover, *JPT2* overexpression further enhanced macrophage chemotaxis, while *JPT2* knockdown

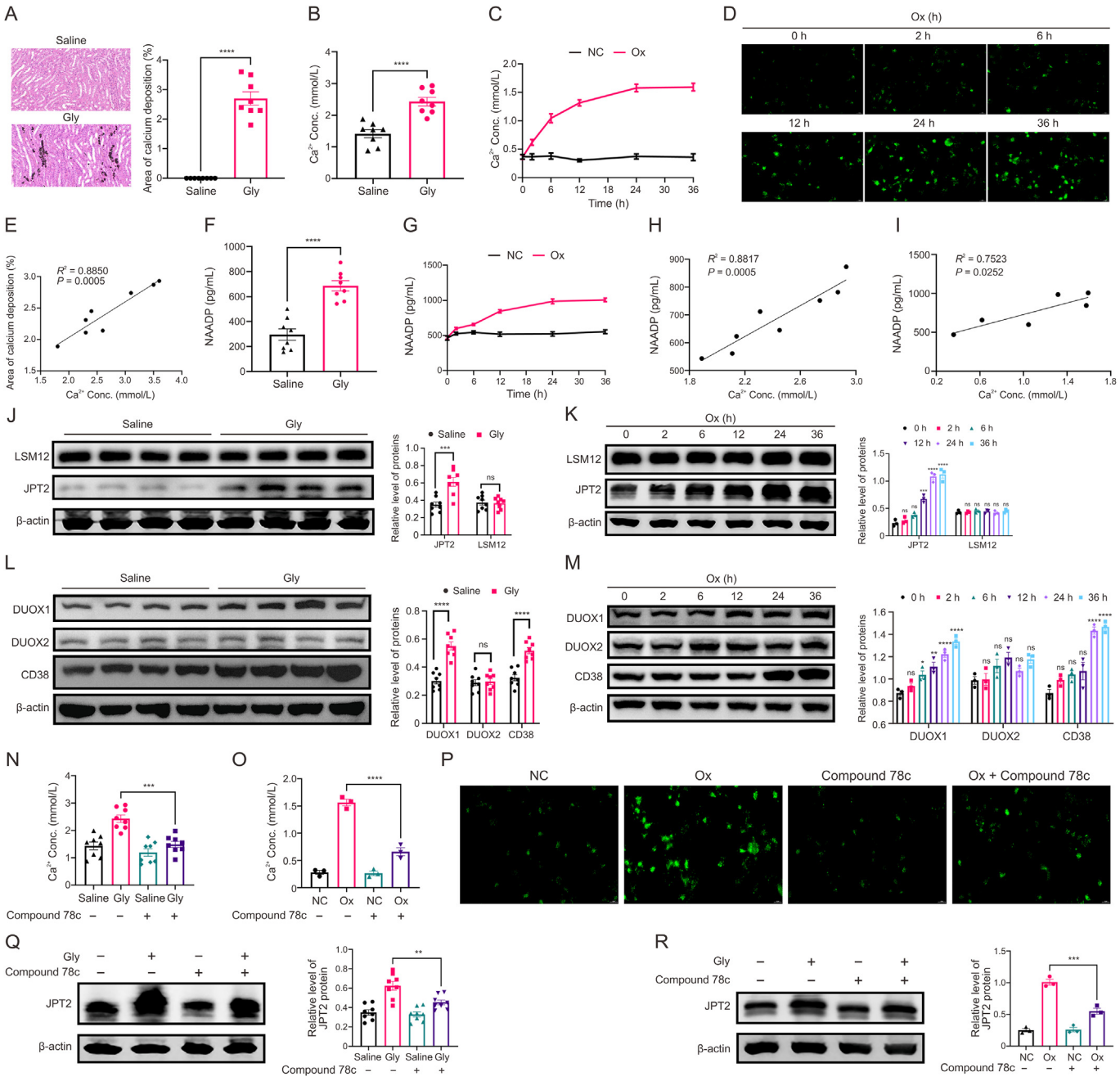

Fig. 1. Oxalate exposure increases the abundance of Jupiter microtubule-associated homolog 2 (JPT2) expression in renal tubular epithelial cells (RTEC) and mice kidneys. (A) The images and quantification of von kossa staining showing calcium oxalate deposition in the kidneys of mice. (B, C) Quantification of Ca^{2+} concentration in mice kidneys (B) and HK-2 cells (C). (D) Representative images of Ca^{2+} fluorescence in oxalate interfered HK-2 cells at specified times by Fluo-3AM. (E) Pearson correlation analysis revealed the correlation between calcium salt deposition and Ca^{2+} concentration in the kidney. (F, G) Quantification of nicotinic acid adenine dinucleotide phosphate (NAADP) concentration in mice kidneys (F) and HK-2 cells (G). (H, I) Correlation analysis of NAADP and Ca^{2+} concentrations in mice kidneys (H) and HK-2 cells (I). (J, K) Representative immunoblots and relative quantification of JPT2 and like-Sm protein 12 (LSM12) protein expression in mice kidneys (J) and HK-2 cells (K) normalized to β-actin. (L, M) Representative immunoblots and relative quantification of dual oxidase 1 (DUOX1), dual oxidase 2 (DUOX2), and CD38 protein expression in mice kidneys (L) and HK-2 cells (M) normalized to β-actin. (N , O) Quantification of Ca^{2+} concentration in the mice kidneys (N) and HK-2 cells (O) treated with compound 78c. (P) Representative images of Ca^{2+} fluorescence in HK-2 cells treated with compound 78c. (Q, R) Representative immunoblots and relative quantification of JPT2 protein expression in the mice kidneys (Q) and HK-2 cells (R) treated with compound 78c normalized to β-actin. The data are shown as mean ± standard error of the mean (SEM). Each data point for *in vivo* experiments represents a mouse, $n = 8$. The data for *in vitro* experiments are from three or four separate experiments, with each data point representing a separate experiment. $^{*}P < 0.05$, $^{**}P < 0.01$, $^{***}P < 0.001$, and $^{****}P < 0.0001$. ns: not significant (versus 0-h group in K and M). Gly: glyoxylate; Ox: oxalate; NC: normal control.

inhibited chemotaxis. In general, macrophages could polarize into classically (M1) or alternatively (M2) activated cells [28]. Kidney stones are associated with M1 macrophages (pro-inflammatory) and the downregulation of M2 macrophages (anti-inflammatory) [27]. The results of qPCR (Figs. 3D and E) showed that the CM derived from HK-2 or HEK-293 cells after oxalate intervention upregulated the expression of M1 macrophage markers (CD86, interleukin (IL)-6, and IL-12) and downregulated the expression of M2 macrophage markers (CD206, IL-10, and CD163). Moreover, *JPT2* overexpression further enhanced M1 macrophage polarization, while *JPT2* knockdown inhibited M1 macrophage polarization. The results of CD86 and CD68 dual fluorescence (Figs. 3F and S3C)

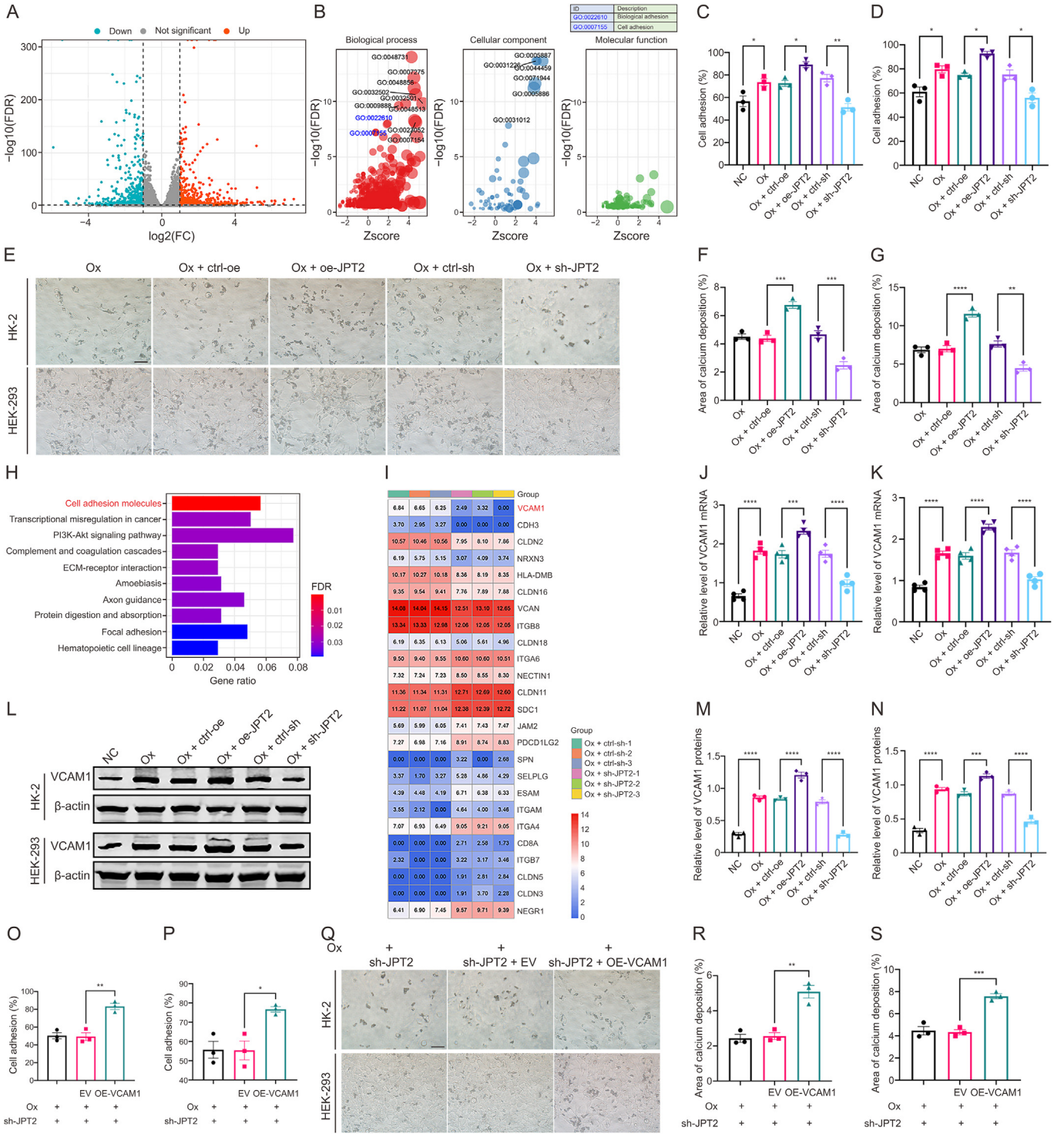

Fig. 2. Jupiter microtubule-associated homolog 2 (JPT2) promotes crystal-cell adhesion caused by oxalate exposure. (A) The volcano plot showing the differentially expressed genes in HK-2 cells of *JPT2* knockdown and control after 24 h of oxalate treatment. (B) The gene ontology (GO) bubble diagram showing the functional annotation of the differential gene enrichment in (A). (C, D) Quantification of cell adhesion capacity assay in HK-2 (C) and HEK-293 cells (D). (E–G) The crystal-cell adhesion images and quantification of HK-2 (E, F) and HEK-293 cells (E, G). (H) The Kyoto Encyclopedia of Genes and Genomes (KEGG) bar plot displaying the functional annotation of differential gene enrichment in (A). (I) The heatmap displaying the differential expression of genes enriched in cell adhesion molecules in (H). (J, K) Quantification of mRNA expression of vascular cell adhesion molecule 1 (VCAM1) in HK-2 (J) and HEK-293 cells (K) normalized to β-actin. (L–N) Representative immunoblots and relative quantification of VCAM1 protein expression in HK-2 (L, M) and HEK-293 cells (L, N) normalized to β-actin. (O, P) Quantification of cell adhesion capacity after knockdown of *VCAM1* in HK-2 (O) and HEK-293 cells (P). (Q–S) Images and quantification of crystal-cell adhesion after knockdown of *VCAM1* in HK-2 (Q, R) and HEK-293 cells (Q, S). These data are expressed as mean ± standard error of the mean (SEM). The data for *in vitro* experiments are from three or four separate experiments, with each data point representing a separate experiment. $^{*}P < 0.05$, $^{**}P < 0.01$, $^{***}P < 0.001$ and $^{****}P < 0.0001$. Ox: oxalate; Ctrl: control; PI3K: phosphatidylinositol 3-kinase; EV: empty vector.FDR: false discovery rate; FC: fold change.

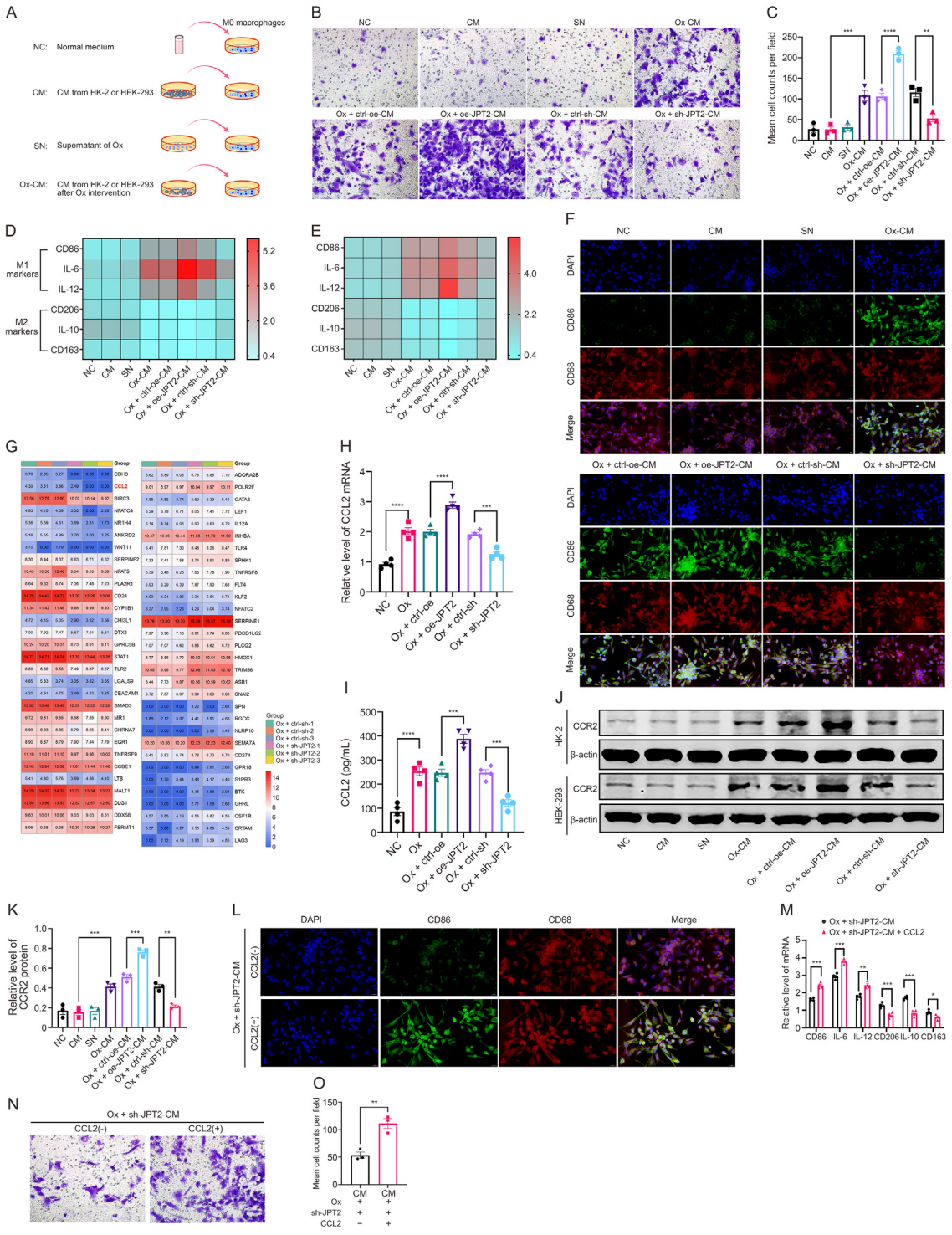

Fig. 3. Jupiter microtubule-associated homolog 2 (JPT2) promotes oxalate-induced macrophage chemotaxis and inflammatory polarization. (A) The intervention pattern of macrophages. (B) Images (B) and quantification (C) of macrophage chemotaxis after intervention with conditioned medium (CM) of HK-2 cells. (D, E) The mRNA expression of CD86, interleukin (IL)-6, IL-12, CD206, IL-10, and CD163 in macrophages after intervention with CM of HK-2 (D) and HEK-293 (E) cells. (F) Immunofluorescence images with CD68 (red) and CD86 (green) after intervention with CM of HK-2 cells. (G) The heatmap showing the differential expression of genes enriched for functions related to cytokine and chemokine production. (H) Quantification of C–C motif chemokine ligand 2 (CCL2) mRNA expression after knockdown and overexpression of *JPT2* in HK-2 cells. (I) Quantification of CCL2 concentration in CM after knockdown and overexpression of *JPT2* in HK-2 cells. (J) Representative immunoblots of CCR2 protein expression in macrophages after intervention with CM of HK-2 and HEK-293 cells. (K) Relative quantification of CCR2 protein expression in macrophages after intervention with CM of HK-2 cells normalized to β-actin. (L) Immunofluorescence images with CD68 (red) and CD86 (green) after intervention with CM of HK-2 cells. (M) The mRNA expression of CD86, IL-6, IL-12, CD206, IL-10, and CD163 in macrophages after intervention with CM of HK-2 cells. (N, O) Images (N) and quantification (O) of macrophage chemotaxis after intervention with CM of HK-2 cells and CCL2. The data are shown as mean ± standard error of the mean (SEM). The data for *in vitro* experiments are from three or four separate experiments, with each data point representing a separate experiment. $^{*}P < 0.05$, $^{**}P < 0.01$, $^{***}P < 0.001$ and $^{****}P < 0.0001$. NC: normal control; DAPI: 4',6-diamidino-2-phenylindole.

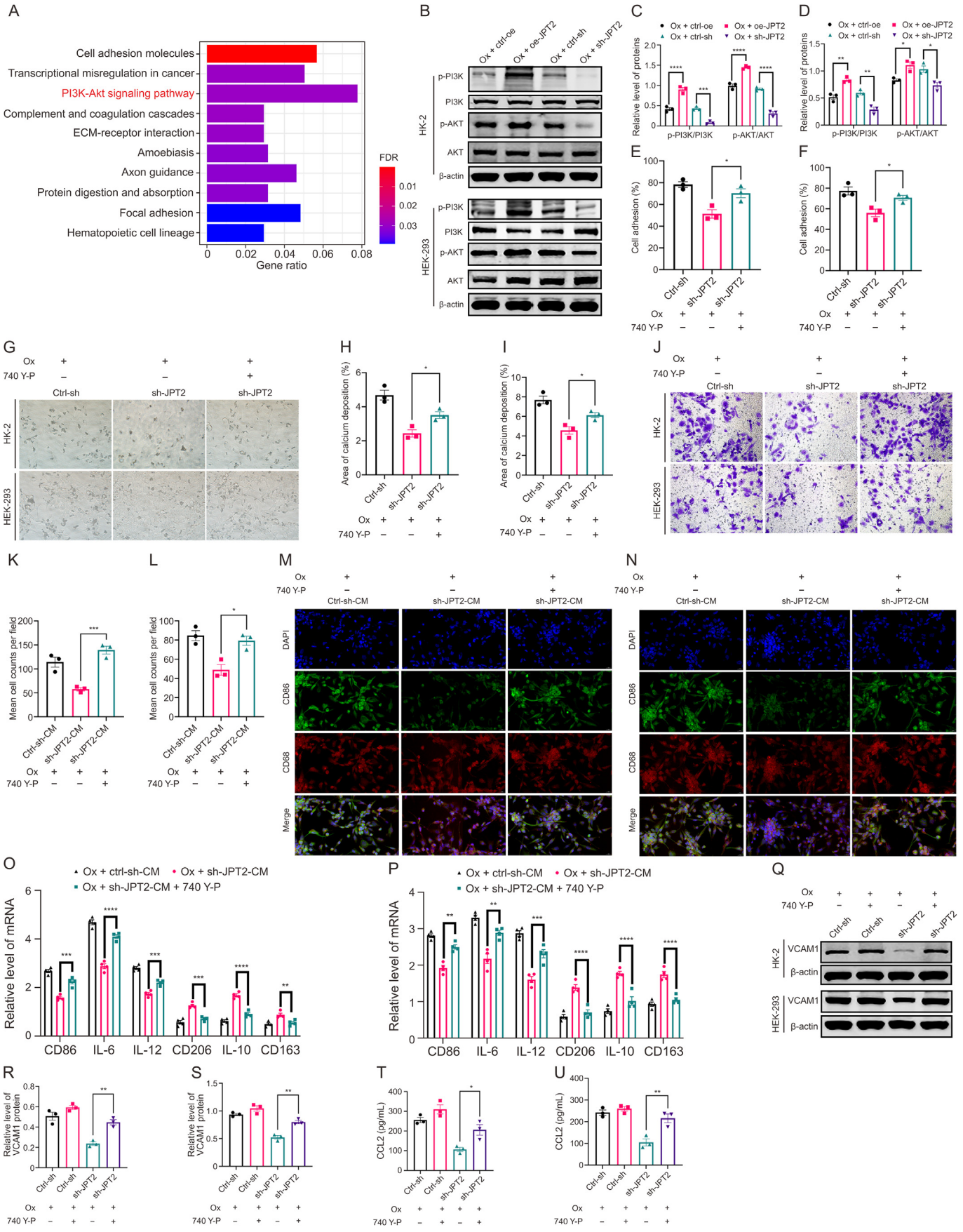
A
Cell adhesion molecules
Transcriptional misregulation in cancer
PI3K-Akt signaling pathway
Complement and coagulation cascades
ECM-receptor interaction
Amoebiasis
Axon guidance
Protein digestion and absorption
Focal adhesion
Hematopoietic cell lineage
Gene ratio
FDR
B
Ox + ctrl-oe
Ox + oe-JPT2
Ox + ctrl-sh
Ox + sh-JPT2
HK-2
HEK-293
p-PI3K
PI3K
p-AKT
AKT
β-actin
C
Relative level of proteins
p-PI3K/PI3K
p-AKT/AKT
D
E
Cell adhesion (%)
Ctrl-sh
sh-JPT2
Ox
740 Y-P
F
G
H
Area of calcium deposition (%)
I
J
K
Mean cell counts per field
Ctrl-sh-CM
sh-JPT2-CM
L
M
Ctrl-sh-CM
sh-JPT2-CM
DAPI
CD86
CD68
Merge
N
O
Ox + ctrl-sh-CM
Ox + sh-JPT2-CM
Ox + sh-JPT2-CM + 740 Y-P
Relative level of mRNA
CD86
IL-6
IL-12
CD206
IL-10
CD163
P
Q
VCAM1
β-actin
R
Relative level of VCAM1 protein
S
T
CCL2 (pg/mL)
U

confirmed the M1 macrophage polarization. Then, to investigate the underlying mechanisms of macrophage chemotaxis and M1 polarization, we selected genes from GO enriched in cytokine production, regulation of cytokine production, cytokine production involved in immune response, regulation of chemokine production, and chemokine production. It was then found that C−C motif chemokine ligand 2 (CCL2) was the most differential chemokine (Fig. 3G). CCL2 is expressed in various endothelial cells, epithelial cells, and tumor cells, and acts by vigorously recruiting various immune cells [29,30]. Additional evidence shows that CCL2 expression is significantly increased in renal papillae and urine in patients with renal stones compared to non-stone patients [31]. Subsequently, we examined the expression and content of CCL2. qPCR (Figs. 3H and S3D) and ELISA results (Figs. 3I and S3E) showed that the expression of CCL2 increased after oxalate intervention, and *JPT2* overexpression increased the expression CCL2. At the same time, *JPT2* knockdown decreased its expression. CCL2 tends to act through its CCR2 [32]. Thus, we further examined CCR2 expression within macrophages. As shown in (Figs. 3J, 3K and S3F), the CM derived from HK-2 or HEK-293 cells after oxalate intervention enhanced CCR2 expression in macrophages, and its expression was further enhanced by *JPT2* overexpression and suppressed by *JPT2* knockdown. We hypothesized that JPT2 regulates macrophage chemotaxis and M1 polarization by affecting CCL2 production in RTEC. Thus, the results of dual fluorescence (Figs. 3L and S3G) and qPCR (Figs. 3M and S3H) showed that adding exogenous CCL2 significantly rescued M1 macrophage polarization that was impaired by JPT2 deficiency in RTEC. As shown in (Figs. 3N, 3O, S3I, and S3J), adding exogenous CCL2 significantly rescued macrophage chemotaxis impaired by JPT2 deficiency in RTEC. These data suggested that JPT2 promotes macrophage chemotaxis and inflammatory polarization by upregulating CCL2 expression in RTEC.

3.4. PI3K/AKT signaling is critical for JPT2 exacerbation of crystal-cell adhesion and macrophage inflammatory polarization caused by oxalate exposure

To elucidate the mechanisms by which JPT2 affects VCAM1 and CCL2 in RTEC, KEGG pathway enrichment analysis was performed on the differential genes after JPT2 deficiency. As shown in (Fig. 4A), the PI3K/AKT signaling was significantly enriched. PI3K/AKT signaling is a pivotal signaling pathway regulating various life activities such as cell survival, proliferation, and metabolism [33,34]. There is evidence that activation of PI3K/AKT signaling enhances the expression of VCAM1 [35] and CCL2 [36]. Western blot results (Figs. 4B−D) showed PI3K and AKT phosphorylation in HK-2 and HEK-293 cells, where *JPT2* overexpression significantly enhances their phosphorylation levels, and *JPT2* knockdown significantly inhibits their phosphorylation. Then, 740 Y-P pretreatment was used to agonize PI3K/AKT signaling in HK-2 and HEK-293 cells. The results showed that pretreatment with 740 Y-P significantly rescued the cell adhesion capacity (Figs. 4E and F), cell-crystal adhesion (Figs. 4G−I), macrophage chemotaxis (Figs. 4J−L), and M1 macrophage polarization (Figs. 4M−P) that were diminished due to JPT2 deficiency. Immediately, the expression of VCAM1 and CCL2 was monitored. The results showed that in HK-2 and HEK-293 cells, pretreatment with 740 Y-P significantly rescued the expression of VCAM1 (Figs. 4Q−S) and CCL2 (Figs. 4T and U) inhibited by JPT2 deficiency. The above results suggested that the key to JPT2 deficiency downregulating VCAM1 and CCL2 expression and affecting cell-crystal adhesion and macrophages is probably the inhibition of PI3K/AKT signaling.

3.5. JPT2 in RTEC exacerbates oxalate-induced macrophage inflammatory polarization by promoting 4-aminobutyrate aminotransferase (ABAT) expression in macrophages

It is known that macrophage metabolic activity regulates their polarization and function, and intracellular metabolic reprogramming can confer sufficient energy and metabolites to macrophages to support their polarization and multiple functions [37−39]. Therefore, we performed untargeted metabolomics to analyze the influence of JPT2 deficiency in RTEC on macrophage metabolism. The positive and negative patterns of untargeted metabolomics identified 8631 features, with lipid and lipid-like molecules metabolites being the most abundant at 48.221% (Fig. S4A). The result of principal component analysis (PCA) showed significant differences between the Ox + Ctrl-sh-CM and Ox + sh-JPT2-CM groups (Fig. S4B). The differential metabolites with $P < 0.05$ and variable importance in the projection (VIP) > 1 were subsequently visualized, where differential metabolites with level B(i) and B(ii) were labeled (Figs. S4C and D). Subsequently, metabolic pathway analysis was performed for the differential metabolites. As shown in (Figs. 5A and S4E), alanine, aspartate and glutamate metabolism were the most significant pathways. Then, through the metabolite flow of alanine, aspartate and glutamate metabolic pathways, we identified succinic acid semialdehyde (SSA) as the key metabolite (Fig. S4F). Subsequently, the box plot (Fig. 5B) showed that SSA is significantly decreased for Ox + sh-JPT2-CM compared to Ox + Ctrl-sh-CM. ABAT is a crucial enzyme for the catabolic production of SSA from the inhibitory neurotransmitter gamma-aminobutyric acid [40]. Therefore, we examined ABAT expression in macrophages and found that the CM derived from HK-2 or HEK-293 cells with *JPT2* overexpression after oxalate intervention significantly upregulated mRNA expression (Figs. 5C and D) and protein expression (Fig. 5E) of ABAT in macrophages. In contrast, the opposite was observed for JPT2 deficiency. SSA produces succinate via succinate semialdehyde dehydrogenase [41]. Succinate is thought to be a potent metabolite in innate immune signaling that promotes IL-1β and leads to M1 polarization in macrophages [42,43]. Therefore, we hypothesized that JPT2 deficiency in RTEC increases intracellular succinate production in macrophages leading to M1 macrophage polarization. Subsequently, we performed overexpression of *ABAT* in macrophages and then examined the polarization status of macrophages. The results of dual fluorescence (Figs. 5F and G) and qPCR (Figs. 5H and I) showed that overexpression of *ABAT* reversed the inhibition of M1 macrophage polarization by *JPT2*

Fig. 4. Phosphatidylinositol 3-kinase (PI3K)/AKT signaling is critical for Jupiter microtubule-associated homolog 2 (JPT2) exacerbation of crystal-cell adhesion and macrophage inflammatory polarization caused by oxalate exposure. (A) The Kyoto Encyclopedia of Genes and Genomes (KEGG) bar graph showing the functional annotation of differential gene enrichment. (B−D) Representative immunoblots and relative quantification of p-PI3K, PI3K, p-AKT, and AKT protein expression in oxalate interfered HK-2 (B, C) and HEK-293 cells (B, D) normalized to β-actin. (E , F) Quantification of cell adhesion capacity assay in HK-2 (E) and HEK-293 cell (F) after 740 Y-P treatment. (G−I) Images and quantification of crystal-cell adhesion in HK-2 (G, H) and HEK-293 cells (G, I) after 740 Y-P treatment. (J−L) Images and quantification of macrophage chemotaxis after intervention with conditioned medium (CM) of HK-2 (J, K) and HEK-293 cells (J, L) after 740 Y-P pretreatments. (M, N) Immunofluorescence images with CD68 (red) and CD86 (green) after intervention with CM of HK-2 (M) and HEK-293 cells (N). (O, P) The mRNA expression of CD86, interleukin (IL)-6, IL-12, CD206, IL-10, and CD163 in macrophages after intervention with CM of HK-2 (O) and HEK-293 cells (P). (Q−S) Representative immunoblots and relative quantification of vascular cell adhesion molecule 1 (VCAM1) protein expression in HK-2 (Q, R) and HEK-293 cells (Q, S) after 740 Y-P treatment normalized to β-actin. (T, U) Quantification of CCL2 concentration in CM of HK-2 (T) and HEK-293 cells (U) after 740 Y-P treatment. The data are expressed as mean ± standard error of the mean (SEM). The data for *in vitro* experiments are from three or four separate experiments, with each data point representing a separate experiment. $^{*}P < 0.05$, $^{**}P < 0.01$, $^{***}P < 0.001$ and $^{****}P < 0.0001$. Ox: oxalate; FDR: false discovery rate; Ctrl: control.

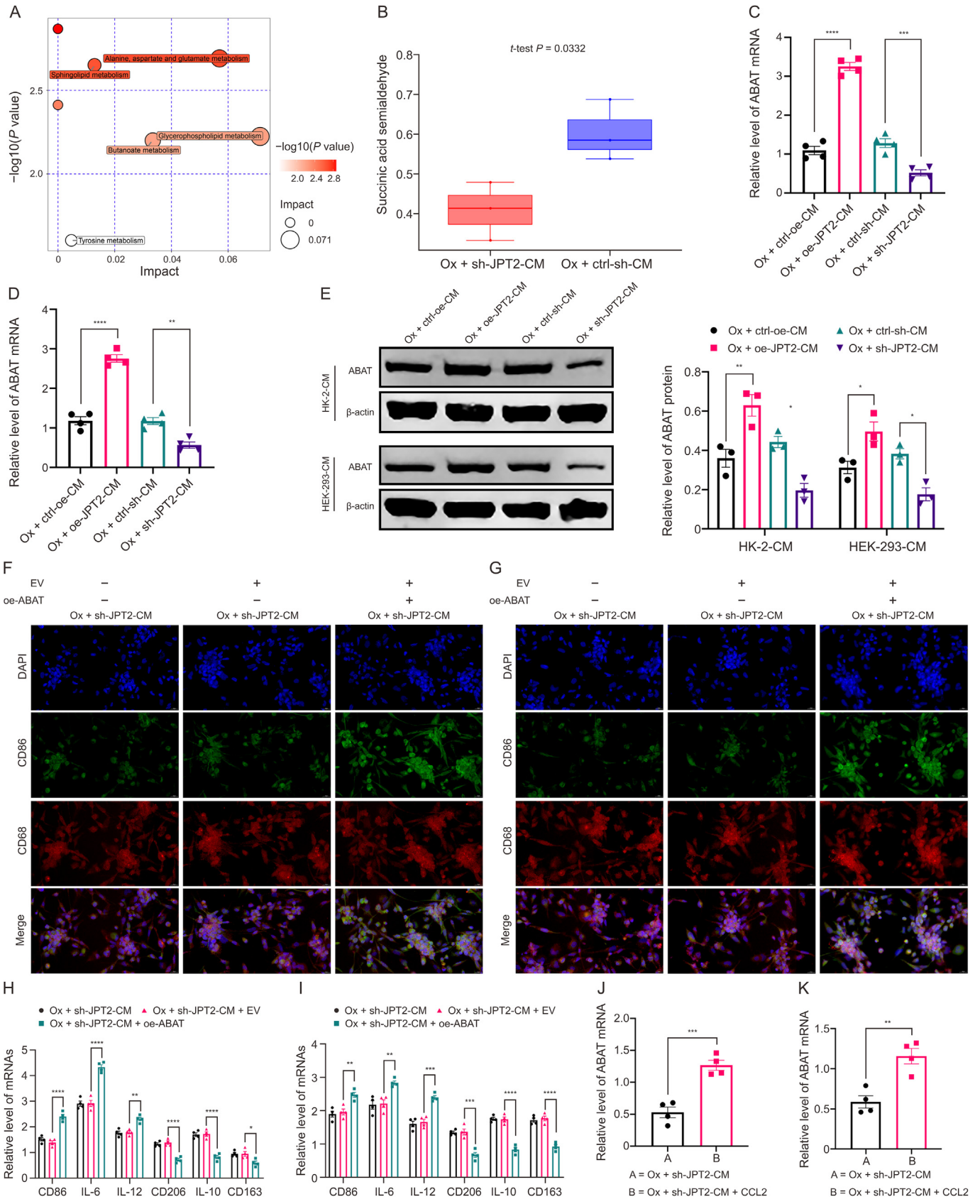

Fig. 5. Jupiter microtubule-associated homolog 2 (JPT2) in renal tubular epithelial cells (RTEC) exacerbates oxalate-induced macrophage inflammatory polarization by promoting 4-aminobutyrate aminotransferase (ABAT) expression in macrophages. (A) The metabolic pathway bubble diagram showing the pathways enriched by differential metabolites. (B) The content of succinic acid semialdehyde (SSA) in groups Ox + Ctrl-sh-CM and Ox + sh-JPT2-CM. (C, D) The mRNA expression of ABAT in macrophages after intervention with conditioned medium (CM) of HK-2 (C) and HEK-293 cells (D). (E) Representative immunoblots and relative quantification of ABAT protein expression in macrophages after

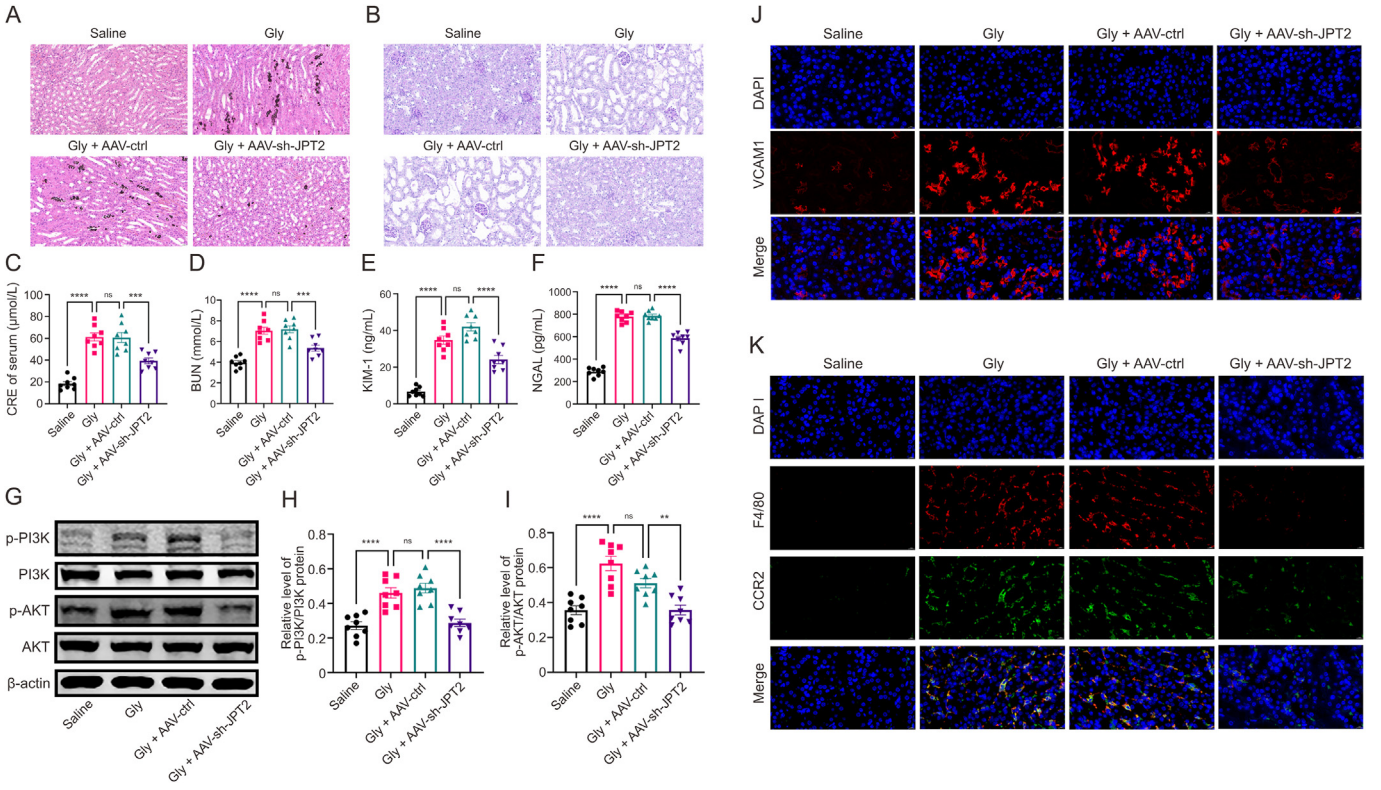

Fig. 6. Jupiter microtubule-associated homolog 2 (JPT2) deficiency attenuates glyoxylate (Gly)-induced kidney calcium oxalate deposition, kidney injury, and macrophage inflammatory activation in mice. (A) The images of von kossa staining showing the degree of kidney calcium oxalate deposition in mice. (B) The images of periodic acid-Schiff (PAS) staining showing the tubular injury in the kidneys. (C, D) Quantification of serum concentrations of creatinine (CRE) (C) and blood urea nitrogen (BUN) (D) showing the degree of kidney injury in mice. (E, F) Quantification of urinary concentrations of kidney injury molecule 1 (KIM-1) (E) and neutrophil gelatinase-associated lipocalin (NGAL) (F) showing the degree of kidney injury in mice. (G–I) Representative immunoblots (G) and relative quantification (H, I) of p-phosphatidylinositol 3-kinase (PI3K), PI3K, p-AKT, and AKT protein expression in the mice kidney. (J) Representative fluorescent images showing vascular cell adhesion molecule 1 (VCAM1) expression in the mice kidney. (K) Representative immunofluorescence images stained with F4/80 (red) and CCR2 (green) showing CCR2 expression of macrophages in the mice kidney. The data are shown as mean ± standard error of the mean (SEM). Each data point for *in vivo* experiments represents a mouse, $n = 8$. $^{**}P < 0.01$, $^{***}P < 0.001$ and $^{****}P < 0.0001$; ns: not significant. Gly: glyoxylate; Ctrl: control; DAPI: 4',6-diamidino-2-phenylindole.

knockdown in RTEC. Then, to further verify that JPT2 deficiency was exerting downregulation of ABAT through inhibition of CCL2. The ABAT expression in macrophages was examined after adding CCL2 to the CM. qPCR results (Figs. 5J and K) showed that adding CCL2 reversed the CM derived from HK-2 or HEK-293 cells with JPT2 deficiency after oxalate intervention downregulated the ABAT expression in macrophages. These data suggested that JPT2 in RTEC upregulates the production of SSA by increasing the expression of ABAT in macrophages, which in turn leads to increased levels of succinate, thereby exacerbating oxalate-induced inflammatory polarization of macrophages.

3.6. JPT2 deficiency attenuates Gly-induced kidney calcium oxalate deposition, kidney injury, and macrophage inflammatory activation in mice

The function of JPT2 in kidney stones needs to be verified by further *in vivo* experiments (Fig. S5A). The adeno-associated virus (AAV)-sh-JPT2 *in situ* injection created mice with JPT2 deficiency in the kidney (Fig. S5B). First, to determine whether AAV-sh-JPT2 injection affects liver function and oxalate metabolism, we monitored the liver morphology and alanine aminotransferase (ALT), aspartate aminotransferase (AST), and oxalate concentrations in the serum and liver of mice. We found that AAV-sh-JPT2 did not lead to changes in liver morphology (Fig. S5C), and AST, GST, and oxalate (Table S2). Next, we examined the effect of JPT2 deficiency on kidney calcium oxalate deposition. As shown in (Figs. 6A and S5D), JPT2 deficiency significantly reduced Gly-induced kidney calcium oxalate deposition of mice. We also examined the effect of JPT2 deficiency on kidney injury in mice. Thus, the results of urine biochemistry (Table S2), periodic acid-Schiff (PAS) staining (Figs. 6B and S5E), serum creatinine (CRE) (Fig. 6C) and blood urea nitrogen (BUN) (Fig. 6D) in serum, and kidney injury molecule 1 (KIM-1) (Fig. 6E) and neutrophil gelatinase-associated lipocalin (NGAL) (Fig. 6F) in urine indicated that JPT2 deficiency significantly attenuated Gly-induced kidney injury. Subsequently, we further validated the molecular mechanism of JPT2 in kidney stones. PI3K/AKT signaling serves as a crucial mediator of JPT2 action. We found that PI3K/AKT signaling in mice kidneys was activated by the intervention of Gly, and JPT2 deficiency significantly inhibited the activation of PI3K/AKT signaling (Figs. 6G–I). Next, we also found that the expression of VCAM1 (Figs. 6J, S5F, and S5G) and CCL2 (Figs. S5H and I) in mice

intervention with CM of HK-2 and HEK-293 cells. (F, G) Immunofluorescence images with CD68 (red) and CD86 (green) after intervention with CM of HK-2 (F) and HEK-293 cells (G). (H, I) The mRNA expression of CD86, interleukin (IL)-6, IL-12, CD206, IL-10, and CD163 in macrophages after intervention with CM of HK-2 (H) and HEK-293 cells (I). (J, K) The mRNA expression of ABAT in macrophages after intervention with CM of HK-2 (J) and HEK-293 cells (K) and C–C motif chemokine ligand 2 (CCL2). The data are shown as mean ± standard error of the mean (SEM). The data for *in vitro* experiments are from three or four separate experiments, with each data point representing a separate experiment. $^{*}P < 0.05$, $^{**}P < 0.01$, $^{***}P < 0.001$ and $^{****}P < 0.0001$. Ox: oxalate; Ctrl: control; DAPI: 4',6-diamidino-2-phenylindole.

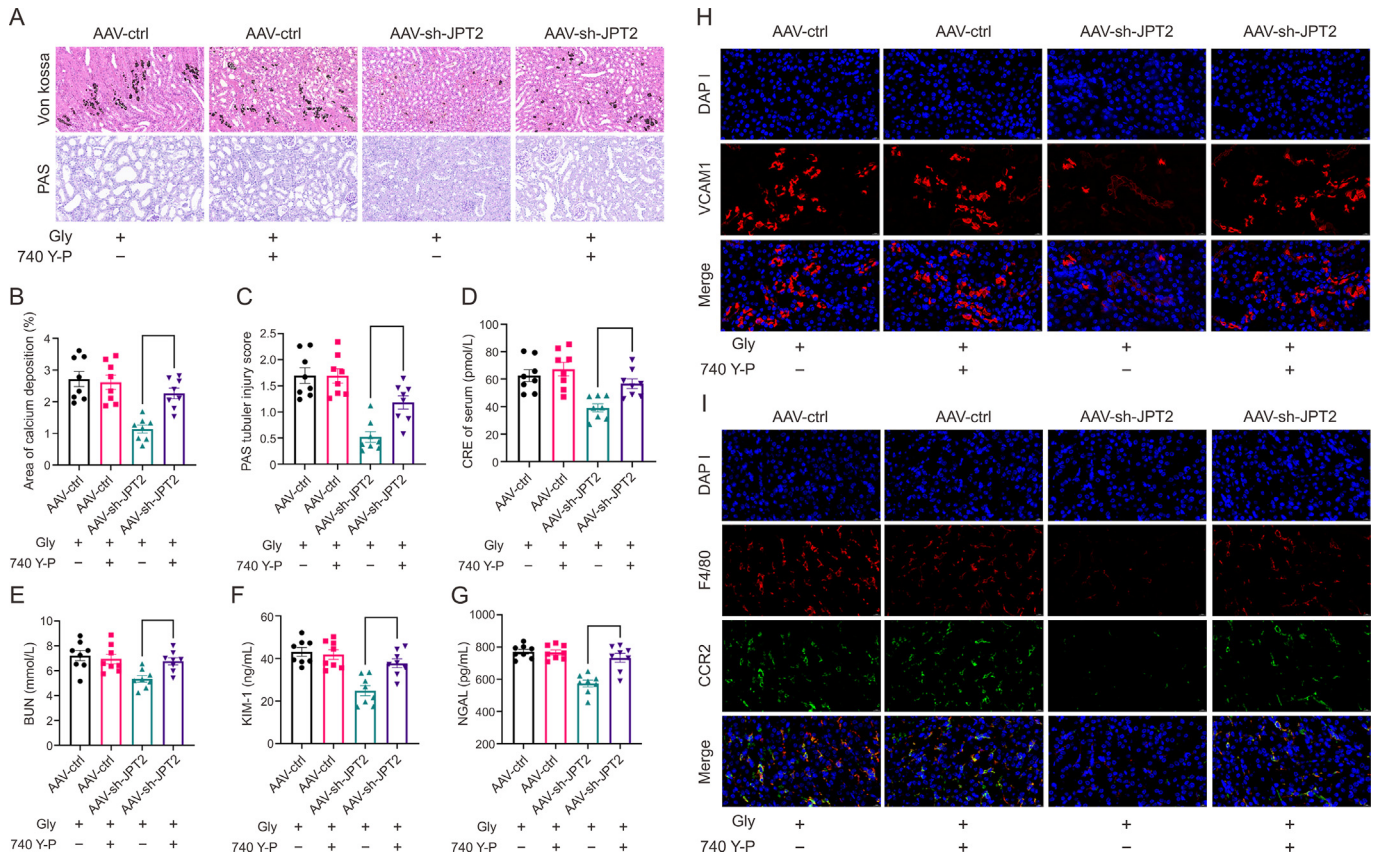

Fig. 7. Phosphatidylinositol 3-kinase (PI3K)/AKT signaling is critical for Jupiter microtubule-associated homolog 2 (JPT2) deficiency in the treatment of glyoxylate (Gly)-induced kidney calcium oxalate deposition, kidney injury, and macrophage inflammatory activation. (A) The images of von kossa and periodic acid-Schiff (PAS) staining showing the degree of kidney calcium oxalate deposition and tubular injury in mice. (B) Quantification of von kossa staining showing the degree of kidney calcium oxalate deposition in mice. (C) Quantification of PAS staining showing the tubular injury in the kidneys. (D, E) Quantification of serum concentrations of creatinine (CRE) (D) and blood urea nitrogen (BUN) (E) showing the degree of kidney injury in mice. (F, G) Quantification of urinary concentrations of kidney injury molecule 1 (KIM-1) (F) and neutrophil gelatinase-associated lipocalin (NGAL) (G) showing the degree of kidney injury in mice. (H) Representative fluorescent images showing vascular cell adhesion molecule 1 (VCAM1) expression in the mice kidney. (I) Representative immunofluorescence images stained with F4/80 (red) and CCR2 (green) showing CCR2 expression of macrophages in the mice kidney. The data are shown as mean ± standard error of the mean (SEM). Each data point for *in vivo* experiments represents a mouse, $n = 8$. $^{*}P < 0.05$, $^{**}P < 0.01$, and $^{****}P < 0.0001$. DAPI: 4',6-diamidino-2-phenylindole.

kidneys was also significantly increased in the kidney stones model. At the same time, JPT2 deficiency significantly inhibited their expression. In addition, the expression of CCR2 (Fig. 6K) and the degree of inflammatory polarization (Fig. S5J) in macrophages of mice kidneys were found to be significantly increased in the kidney stones model constructed with Gly, and JPT2 deficiency significantly inhibited the expression of CCR2 and the degree of inflammatory polarization in macrophages increased by Gly. Finally, we also validated the metabolic mechanism of JPT2 in the kidney stones model. The results of serum and kidney biochemical assays (Table S2) showed that Gly significantly increased the levels of oxalate in serum, as well as the levels of citrate and succinate in kidneys, but did not significantly alter citrate and succinate in serum. JPT2 deficiency significantly decreased the levels of succinate in kidneys, but did not significantly alter oxalate and citrate. This may imply that JPT2 deficiency has some effect on succinate in kidney macrophages within the metabolic machinery, but does not affect oxalate and citrate metabolism in the kidney and systemically. In addition, since JPT2 is activated by NAADP in kidney stones, we sought to compare the efficacy of NAADP inhibition and JPT2 deficiency on kidney stones. The results showed that inhibition of NAADP similarly attenuated kidney calcium oxalate deposition (Figs. S6A and B) and kidney injury (Figs. S6C–F) to some extent, but was not as efficacious as directly targeting JPT2. These data demonstrated that JPT2 deficiency attenuates oxalate-induced kidney calcium oxalate deposition, kidney injury, and macrophage inflammatory activation.

3.7. PI3K/AKT signaling is critical for JPT2 deficiency in the treatment of Gly-induced kidney calcium oxalate deposition, kidney injury, and macrophage inflammatory activation

To determine the role of PI3K/AKT signaling in JPT2 influence on kidney stones, we intervened in JPT2 deficient mice using agonists of PI3K/AKT signaling and monitored indicators of kidney stones. The results revealed that 740Y-P significantly reversed kidney calcium oxalate deposition (Figs. 7A and B), kidney injury (Figs. 7A and C–G), and macrophage inflammatory activation (Fig. S7A) inhibited by JPT2 deficiency. And, mechanistically, 740Y-P significantly reversed the expression of VCAM1 (Figs. 7H, S7B, and S7C), CCL2 (Figs. S7D and E) in RTEC and CCR2 (Fig. 7I) in macrophages inhibited by JPT2 deficiency. These data suggested that PI3K/AKT signaling is the critical bridge for the treatment of kidney stones in JPT2 deficiency.

4. Discussion

Supraphysiologic concentrations of oxalate cause metabolic burden in the body. The kidneys are an important excretion route for oxalates that are absorbed into the bloodstream, which may

lead to kidney stones. Kidney stones are characterized by pathological mineralization due to an aberrant urinary environment and chronic inflammation, in which an imbalance of Ca^{2+} homeostasis in RTEC is essential for microcalcification of kidney stones and urinary crystal formation [44,45]. Therefore, in view of the toxic effects of oxalate and calcium homeostatic imbalance on kidney stones, it is important to study the role of oxalate exposure and calcium homeostatic imbalance in the mineralization of kidney stones for their prevention and treatment.

NAADP is a crucial regulatory molecule of intracellular Ca^{2+} mobilization, which exerts Ca^{2+} mobilization and signal amplification by forming a codependent complex with JPT2 or LSM12 [11,46]. Here, we found that oxalate exposure increased NAADP, calcium concentration, and protein expression of JPT2 on HK-2 and HEK-293 cells, but no change in LSM12 expression. Therefore, we suggest that JPT2 is the binding protein of NAADP in the kidney stones model. Together, NAADP/JPT2-mediated Ca^{2+} mobilization may contribute to the pathogenesis of kidney stones.

Here, the biological behavior of cell adhesion was enriched in JPT2 deficient HK-2 as detected by transcriptomic analysis. Crystal-cell adhesion has been reported to be involved in the entire pathology of kidney stones as an essential part of the vicious cycle [47–49]. We found that VCAM1 is a crucial molecule of JPT2 affecting crystal-cell adhesion, which is accompanied by the downregulation of JPT2. VCAM1 is an essential cell adhesion molecule [50]. It was reported that VCAM1 expression was significantly increased in magnesium ammonium phosphate stones [51]. This is consistent with our findings.

It was reported that the expression of inflammation-related genes in kidney stones induces macrophage migration and phagocytosis [52,53]. Similar to these results, our investigations also showed that the CM of RTEC with JPT2 deficiency inhibits macrophage chemotaxis and inflammatory polarization. It has been reported that CCL2 promotes macrophage chemotaxis and inflammatory polarization [54,55]. Our study similarly confirmed that adding CCL2 could reverse the macrophage chemotaxis and inflammatory polarization attenuated by JPT2-deficient RTEC-derived CM. Thus, CCL2 was essential for JPT2 deficiency in RTEC to influence macrophage chemotaxis.

There were reports that PI3K/AKT signaling was significantly activated in kidney stones [56]. Here, the transcriptomic analysis indicated that PI3K/AKT signaling was enriched considerably, and subsequent western blot results showed that JPT2 deficiency significantly inhibited PI3K and AKT phosphorylation in RTEC. Additional evidence showed that activation of PI3K/AKT signaling enhanced the expression of VCAM1 [35] and CCL2 [36]. Similarly, our experiments showed that agonists of PI3K significantly reversed the expression of VCAM1 and CCL2 downregulation due to JPT2 deficiency. However, the underlying mechanism through which JPT2 affects the phosphorylation of PI3K/AKT signaling in kidney stones remains to be further elucidated.

Macrophage function is influenced by cellular metabolism [57]. The untargeted metabolomic analysis demonstrated that JPT2 deficiency in RTEC caused decreased SSA in macrophages, and the SSA product succinate enhances the inflammatory polarization of macrophages [58]. Thus, it is tempting to conclude that JPT2 deficiency in RTEC reduces SSA production by suppressing ABAT expression, further inhibiting succinate production and thus blocking macrophage inflammatory polarization. This speculation was verified by the reversal of macrophage inflammatory polarization impeded by JPT2 deficiency in RTEC through overexpression of ABAT. We also demonstrated that JPT2 deficiency affects ABAT expression in macrophages by inhibiting CCL2 secretion using remedial experiments on ABAT expression by CCL2.

The results of *in vivo* experiments further confirmed that JPT2 deficiency ameliorates Gly-induced kidney calcium oxalate deposition, kidney injury, and macrophage inflammatory activation in mice. Notably, we found that Gly increased kidney succinate levels and decreased citrate levels, which seems inconsistent with the position of succinate and citrate in the tricarboxylic acid cycle. JPT2 deficiency inhibits succinate levels but fails to alter citrate. This implies that citrate metabolism in kidney stones may be regulated by other potential mechanisms, while succinate metabolism is likely related to the macrophage regulatory mechanism of JPT2. Moreover, the activator of PI3K/AKT signaling was able to significantly reverse the excellent stones treatment ability brought about by JPT2 deficiency. However, since JPT2 deficiency and PI3K/AKT activation in mice is not targeted to RTEC and macrophages are implicated, the potential effects caused by JPT2 deficiency or PI3K/AKT activation in macrophages or other cells cannot be completely ruled out in this study.

5. Conclusion

The intrinsic link between oxalate exposure and kidney stones has long been held by urologists, and unraveling the pathologic mechanisms involved would be a tremendous boost to pharmaceutical development for kidney stones. In conclusion, we show for the first time that oxalate exposure promotes crystal-cell adhesion and regulates macrophage metabolism and inflammatory polarization through JPT2/PI3K/AKT signaling. Based on our findings, JPT2 may be crucial for the mineralization mechanism of kidney stones caused by oxalate exposure, which provides a potential target for treating and diagnosing kidney stones.

CRediT author statement

Qianlin Song: Visualization, Data curation, Formal analysis, Visualization, Writing - Original draft preparation, and Reviewing and Editing; **Chao Song**: Data curation, Formal analysis, and Writing - Original draft preparation; **Xin Chen**: Methodology, Software, Supervision, Validation, and Visualization. **Yunhe Xiong**: Project administration, and Investigation; **Ziqi He**: Data curation; **Xiaozhe Su**: Formal analysis; **Jiawei Zhou**: Resources; **Hu Ke**: Validation; **Caitao Dong**: Visualization; **Wenbiao Liao**: Conceptualization, Writing - Reviewing and Editing, Supervision, and Funding acquisition; **Sixing Yang**: Conceptualization, Writing - Reviewing and Editing, Project administration, Resources, and Funding acquisition.

Declaration of competing interest

The authors declare that there are no conflicts of interest.

Acknowledgments

This work was supported by the National Natural Science Foundation of China (Grant Nos.: 82070723, and 82270797) and Nature Science Foundation of Hubei Province, China (Grant No.: 2022CFC020).

Appendix A. Supplementary data

Supplementary data to this article can be found online at https://doi.org/10.1016/j.jpha.2024.02.010.

References

[1] M. Bargagli, M.C. Tio, S.S. Waikar, et al., Dietary oxalate intake and kidney outcomes, Nutrients 12 (2020), 2673.
[2] B. Misiewicz, D. Mencer, W. Terzaghi, et al., Analytical methods for oxalate quantification: The ubiquitous organic anion, Molecules 28 (2023), 3206.
[3] C. Li, L. Wang, M. Yuan, et al., A new route for indirect mineralization of carbon dioxide-sodium oxalate as a detergent builder, Sci. Rep. 9 (2019), 12852.
[4] Y. Wang, C.J.E. Davey, K. van der Maas, et al., Biodegradability of novel high T_g poly(isosorbide-co-1,6-hexanediol) oxalate polyester in soil and marine environments, Sci. Total Environ. 815 (2022), 152781.
[5] M. Liebman, I.A. Al-Wahsh, Probiotics and other key determinants of dietary oxalate absorption, Adv. Nutr. 2 (2011) 254–260.
[6] C. Witting, C.B. Langman, D. Assimos, et al., Pathophysiology and treatment of enteric hyperoxaluria, Clin. J. Am. Soc. Nephrol. 16 (2021) 487–495.
[7] C. Thongprayoon, A.E. Krambeck, A.D. Rule, Determining the true burden of kidney stone disease, Nat. Rev. Nephrol. 16 (2020) 736–746.
[8] M.S.C. Morgan, M.S. Pearle, Medical management of renal stones, BMJ 352 (2016), i52.
[9] Y. Yang, Y. Deng, Y. Wang, Major geogenic factors controlling geographical clustering of urolithiasis in China, Sci. Total Environ. 571 (2016) 1164–1171.
[10] G.S. Gunaratne, E. Brailoiu, S. He, et al., Essential requirement for JPT2 in NAADP-evoked Ca^{2+} signaling, Sci. Signal. 14 (2021), eabd5605.
[11] T.F. Walseth, A.H. Guse, NAADP: From discovery to mechanism, Front. Immunol. 12 (2021), 703326.
[12] J.S. Marchant, G.S. Gunaratne, X. Cai, et al., NAADP-binding proteins find their identity, Trends Biochem. Sci. 47 (2022) 235–249.
[13] M.J. Berridge, M.D. Bootman, H.L. Roderick, Calcium signalling: Dynamics, homeostasis and remodelling, Nat. Rev. Mol. Cell Biol. 4 (2003) 517–529.
[14] A.J. Branco, A.S. Vattamparambil, G.M. Landry, Lead (Pb^{2+})-induced calcium oxalate crystallization ex vivo is ameliorated via inositol 1,4,5-trisphosphate receptor ($InsP_3R$) knockdown in a Drosophila melanogaster model of nephrolithiasis, Environ. Toxicol. Pharmacol. 87 (2021), 103695.
[15] Q. Song, C. Song, X. Chen, et al., FKBP5 deficiency attenuates calcium oxalate kidney stone formation by suppressing cell-crystal adhesion, apoptosis and macrophage M1 polarization via inhibition of NF-κB signaling, Cell Mol. Life Sci. 80 (2023), 301.
[16] X. Feng, L. Chen, W. Guo, et al., Graphene oxide induces p62/SQSTM-dependent apoptosis through the impairment of autophagic flux and lysosomal dysfunction in PC12 cells, Acta Biomater. 81 (2018) 278–292.
[17] A.W. Miller, D. Choy, K.L. Penniston, et al., Inhibition of urinary stone disease by a multi-species bacterial network ensures healthy oxalate homeostasis, Kidney Int. 96 (2019) 180–188.
[18] K.Y. Renkema, K. Lee, C.N. Topala, et al., TRPV5 gene polymorphisms in renal hypercalciuria, Nephrol, Dial. Transplant. 24 (2009) 1919–1924.
[19] W. Wang, B. Qian, C. Zhao, et al., Sublytic C5b-9 Induces CCL3/4 production and macrophage accumulation in thy-1N rats via PKC-α/p65/IRF-8 axis, Int. J. Biol. Sci. 18 (2022) 3178–3193.
[20] H. Liu, X. Yang, K. Tang, et al., Sulforaphane elicts dual therapeutic effects on renal inflammatory injury and crystal deposition in calcium oxalate nephrocalcinosis, Theranostics. 10 (2020) 7319–7334.
[21] A.H. Guse, B.P. Diercks, Integration of nicotinic acid adenine dinucleotide phosphate (NAADP)-dependent calcium signalling, J. Physiol. 596 (2018) 2735–2743.
[22] F. Gu, A. Krüger, H.G. Roggenkamp, et al., Dual NADPH oxidases DUOX1 and DUOX2 synthesize NAADP and are necessary for Ca^{2+} signaling during T cell activation, Sci. Signal. 14 (2021), eabe3800.
[23] C.D. Haffner, J.D. Becherer, E.E. Boros, et al., Discovery, synthesis, and biological evaluation of thiazoloquin(az)olin(on)es as Potent CD38 Inhibitors, J. Med. Chem. 58 (2015) 3548–3571.
[24] W. Li, F. Yan, H. Zhou, et al., P. aeruginosa lipopolysaccharide-induced MUC5AC and CLCA3 expression is partly through Duox1 in vitro and in vivo, PLoS One 8 (2013), e63945.
[25] L. Zhong, M.J. Simard, J. Huot, Endothelial microRNAs regulating the NF-κB pathway and cell adhesion molecules during inflammation, FASEB J. 32 (2018) 4070–4084.
[26] M. Rafat, L.S. Rotenstein, J.L. Hu, et al., Engineered endothelial cell adhesion via VCAM1 and E-selectin antibody-presenting alginate hydrogels, Acta Biomater. 8 (2012) 2697–2703.
[27] S.R. Khan, B.K. Canales, P.R. Dominguez-Gutierrez, Randall's plaque and calcium oxalate stone formation: Role for immunity and inflammation, Nat. Rev. Nephrol. 17 (2021) 417–433.
[28] J. Xue, S.V. Schmidt, J. Sander, et al., Transcriptome-based network analysis reveals a spectrum model of human macrophage activation, Immunity 40 (2014) 274–288.
[29] S. Singh, D. Anshita, V. Ravichandiran, MCP-1: Function, regulation, and involvement in disease, Int. Immunopharmacol. 101 (2021), 107598.
[30] X. Li, W. Yao, Y. Yuan, et al., Targeting of tumour-infiltrating macrophages via CCL2/CCR2 signalling as a therapeutic strategy against hepatocellular carcinoma, Gut 66 (2017) 157–167.
[31] A.Y. Sun, B. Hinck, B.R. Cohen, et al., Inflammatory cytokines in the papillary tips and urine of nephrolithiasis patients, J. Endourol. 32 (2018) 236–244.
[32] I. Conti, B.J. Rollins, CCL2 (monocyte chemoattractant protein-1) and cancer, Semin. Cancer Biol. 14 (2004) 149–154.
[33] J. Wang, K. Hu, X. Cai, et al., Targeting PI3K/AKT signaling for treatment of idiopathic pulmonary fibrosis, Acta Pharm. Sin. B. 12 (2022) 18–32.
[34] J. Yang, J. Nie, X. Ma, et al., Targeting PI3K in cancer: mechanisms and advances in clinical trials, Mol. Cancer. 18 (2019), 26.
[35] X. Li, W. Chen, P. Li, et al., Follicular stimulating hormone accelerates atherogenesis by increasing endothelial VCAM-1 expression, Theranostics. 7 (2017) 4671–4688.
[36] T. Kasemsuk, S. Phuagkhaopong, R. Yubolphan, et al., Cadmium induces CCL2 production in glioblastoma cells via activation of MAPK, PI3K, and PKC pathways, J. Immunotoxicol. 17 (2020) 186–193.
[37] J. Yan, T. Horng, Lipid metabolism in regulation of macrophage functions, Trends Cell Biol. 30 (2020) 979–989.
[38] J. Van den Bossche, L.A. O'Neill, D. Menon, Macrophage immunometabolism: Where are we (going)? Trends Immunol. 38 (2017) 395–406.
[39] W. He, A. Heinz, D. Jahn, et al., Complexity of macrophage metabolism in infection, Curr. Opin. Biotechnol. 68 (2021) 231–239.
[40] A. Besse, P. Wu, F. Bruni, et al., The GABA transaminase, ABAT, is essential for mitochondrial nucleoside metabolism, Cell Metab. 21 (2015) 417–427.
[41] P. Malaspina, M.J. Picklo, C. Jakobs, et al., Comparative genomics of aldehyde dehydrogenase 5a1 (succinate semialdehyde dehydrogenase) and accumulation of gamma-hydroxybutyrate associated with its deficiency, Hum. Genomics. 3 (2009) 106–120.
[42] E.L. Mills, B. Kelly, A. Logan, et al., Succinate dehydrogenase supports metabolic repurposing of mitochondria to drive inflammatory macrophages, Cell 167 (2016) 457–470 e13.
[43] G.M. Tannahill, A.M. Curtis, J. Adamik, et al., Succinate is an inflammatory signal that induces IL-1β through HIF-1α, Nature 496 (2013) 238–242.
[44] C.L. Ibeh, A.J. Yiu, Y.L. Kanaras, et al., Evidence for a regulated Ca^{2+} entry in proximal tubular cells and its implication in calcium stone formation, J. Cell Sci. 132 (2019), jcs225268.
[45] S. Shin, C.L. Ibeh, E. Awuah Boadi, et al., Hypercalciuria switches Ca^{2+} signaling in proximal tubular cells, induces oxidative damage to promote calcium nephrolithiasis, Genes Dis. 9 (2021) 531–548.
[46] S. Patel, G.S. Gunaratne, J.S. Marchant, et al., NAADP receptors: A one-two, Cell Calcium 100 (2021), 102478.
[47] S.R. Khan, M.S. Pearle, W.G. Robertson, et al., Kidney stones, Nat. Rev. Dis. Primers 2 (2016), 16008.
[48] Y. Li, X. Lu, Z. Yu, et al., Meta-data analysis of kidney stone disease highlights ATP1A1 involvement in renal crystal formation, Redox Biol. 61 (2023), 102648.
[49] X. Sheng, T. Jung, J.A. Wesson, et al., Adhesion at calcium oxalate crystal surfaces and the effect of urinary constituents, Proc. Natl. Acad. Sci. USA 102 (2005) 267–272.
[50] J.A. Boyce, E.A. Mellor, B. Perkins, et al., Human mast cell progenitors use alpha4-integrin, VCAM-1, and PSGL-1 E-selectin for adhesive interactions with human vascular endothelium under flow conditions, Blood 99 (2002) 2890–2896.
[51] R.N. Liu, D.M. Zou, M.Y. Tian, et al., Effect of magnesium ammonium phosphate on the expression of adhesion molecules in sheep renal tubular epithelial cells, Res. Vet. Sci. 138 (2021) 167–177.
[52] A. Okada, T. Yasui, S. Hamamoto, et al., Genome-wide analysis of genes related to kidney stone formation and elimination in the calcium oxalate nephrolithiasis model mouse: Detection of stone-preventive factors and involvement of macrophage activity, J. Bone Miner. Res. 24 (2009) 908–924.
[53] A. Okada, T. Yasui, Y. Fujii, et al., Renal macrophage migration and crystal phagocytosis via inflammatory-related gene expression during kidney stone formation and elimination in mice: Detection by association analysis of stone-related gene expression and microstructural observation, J. Bone Miner. Res. 25 (2010) 2701–2711.
[54] C. Wei, C. Yang, S. Wang, et al., Crosstalk between cancer cells and tumor associated macrophages is required for mesenchymal circulating tumor cell-mediated colorectal cancer metastasis, Mol. Cancer 18 (2019), 64.
[55] Y. Nio, T. Yamauchi, M. Iwabu, et al., Monocyte chemoattractant protein-1 (MCP-1) deficiency enhances alternatively activated M2 macrophages and ameliorates insulin resistance and fatty liver in lipoatrophic diabetic A-ZIP transgenic mice, Diabetologia. 55 (2012) 3350–3358.
[56] Y. Si, L. Liu, J. Cheng, et al., Oral hydrogen-rich water alleviates oxalate-induced kidney injury by suppressing oxidative stress, inflammation, and fibrosis, Front. Med. 8 (2021), 713536.
[57] L.A.J. O'Neill, E.J. Pearce, Immunometabolism governs dendritic cell and macrophage function, J. Exp. Med. 213 (2016) 15–23.
[58] P.S. Liu, H. Wang, X. Li, et al., α-ketoglutarate orchestrates macrophage activation through metabolic and epigenetic reprogramming, Nat. Immunol. 18 (2017) 985–994.